Stress evolution of the San Andreas fault system: Recurrence interval versus locking depth

Bridget Smith-Konter[1,2] and David Sandwell[1]

[1]   Major ruptures along the San Andreas Fault System (SAFS) are driven by stress that has accumulated in the upper locked portion of the crust. The present-day stress accumulation rate on any given fault segment is fairly well resolved by current geodetic measurements. Model stress accumulation rates vary between 0.5 and 7 MPa per century and are inversely proportional to earthquake recurrence intervals. In contrast, the total accumulated stress on a given fault segment is poorly resolved since it depends on the uncertain rupture history of each fault over the past few thousand years. We simulate accumulated stress at crustal depths for both past and present-day conditions by assuming complete release of accumulated slip deficit during major ruptures. These speculative results indicate that the southern San Andreas, which has not ruptured in a major earthquake in over 300 years, is currently approaching a threshold stress level. **Citation:** Smith-Konter, B., and D. Sandwell (2009), Stress evolution of the San Andreas fault system: Recurrence interval versus locking depth, *Geophys. Res. Lett.*, *36*, L13304, doi:10.1029/2009GL037235.

1.   Introduction

[2]   The most fundamental model for characterizing earthquake occurrence [*Reid*, 1910] assumes a constant stress accumulation rate on a locked fault segment, which eventually fails at a threshold stress level. While this model provides a conceptual framework for investigating the conditions that prepare a fault for failure, there is little evidence that faults rupture periodically [*Weldon et al.*, 2004] or at a uniform threshold stress [*Murray and Segall*, 2002]. Moreover, this model fails to explain the large differences in earthquake recurrence intervals for various segments of major fault systems: why do some faults rupture on the order of 10s of years, while others require 100s of years to accumulate substantial stress before failing in a large earthquake? We are beginning to address this question using the growing archive of geodetic and paleo-seismic measurements situated along the North American-Pacific plate boundary. Geodetic measurements [e.g., *Shen et al.*, 2003] provide a detailed estimate of the present-day surface strain accumulation rate and using a physical model [e.g., *Smith and Sandwell*, 2003, 2006] or interpolation methods [e.g., *Parsons*, 2006; *Freed et al.*, 2007], these

measurements can be converted to stress accumulation rate. When combined with historical and 1000-year paleoseismic chronologies of the San Andreas Fault System (SAFS) [e.g., *Grant and Lettis*, 2002; *Weldon et al.*, 2004, 2005], stress models can critically improve our understanding of earthquake cycle physics along the plate boundary.

2.   Modeling Earthquake Cycle Stress Variations

[3]   To explore stress variations of the SAFS throughout the earthquake cycle, we employ a 4-dimensional kinematic model [*Smith and Sandwell*, 2004, 2006] spanning the North American-Pacific plate boundary that simulates inter-seismic strain accumulation, coseismic displacement, and post-seismic viscous relaxation of the mantle. The plate boundary consists of a series of vertical connected faults embedded in an elastic plate overlying a viscoelastic half-space (Young's modulus $E = 70$ GPa, shear modulus $\mu = 30$ GPa, elastic plate thickness $H = 60$ km, viscosity $\eta = 1 \times 10^{19}$ Pa s, coefficient of friction $\mu_f = 0.6$) [*Fay and Humphreys*, 2005; *Smith and Sandwell*, 2006]. Deep slip along these faults drives the secular interseismic crustal motions and stress accumulation. Long-term slip rates (see auxiliary material)[1] are initially constrained by geologic estimates and then adjusted to also match contemporary geodetic velocities [*Smith and Sandwell*, 2003; *Becker et al.*, 2004; *Meade and Hager*, 2005; *Wdowinski et al.*, 2007]. Geodetically-derived apparent locking depths are also prescribed [*Smith and Sandwell*, 2003, 2006]. Apparent locking depths range between 0 and 26 km (see auxiliary material), are consistent with seismicity depths [e.g., *Eberhart-Phillips et al.*, 1990; *Lyons et al.*, 2002], and provide an rms residual velocity model misfit of 2.9 mm/yr (along-strike) and 1.8 mm/yr (across-strike). Both locking depths and slip rates are critical parameters controlling the present-day stress accumulation rate on active faults.

[4]   The non-secular evolution of stress on each fault segment is primarily determined by the earthquake rupture history on that segment. This history requires knowledge of both the timing of earthquakes over at least the last 1000 years (i.e., multiple earthquake cycles) and the slip distribution along the segment. Except for the more recent instrumentally recorded events, historical slip distribution is usually unknown and paleoseismic earthquake dates and slip are uncertain. In this study, we impose our best estimate of rupture history based on published historical and paleo-seismic events [e.g., *Grant and Lettis*, 2002; *Weldon et al.*, 2005], which total roughly 75 earthquakes (>M6.0) over the past 1000 years [cf. *Smith and Sandwell*, 2006]. We assume

---

[1]Institute for Geophysics and Planetary Physics, Scripps Institution of Oceanography, La Jolla, California, USA.
[2]Now at Department of Geological Sciences, University of Texas at El Paso, El Paso, Texas, USA.
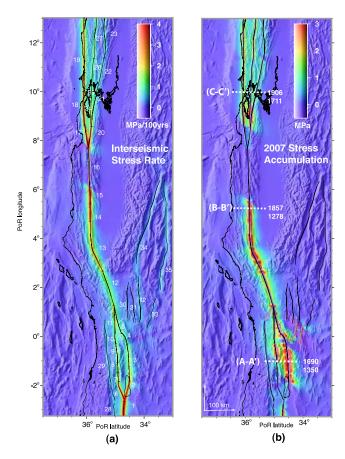

Figure 1. (a) Coulomb stress accumulation rate of the SAFS, evaluated at 1/2 of the locking depth (see auxiliary material), in MPa/100yrs, projected into Pole of Rotation (PoR) coordinate system [*Wdowinski et al.*, 2007]. Color scale is saturated at 4 MPa/100yrs. Labeled numbers correspond to fault segment numbers (see auxiliary material). (b) Present-day (calendar year 2007) Coulomb stress accumulation of the SAFS based on stress accumulation and contributions from 75 historical and prehistorical earthquake ruptures. Segments 30–35 were omitted from the model due to lack of reliable historical data. Color scale is saturated at 3 MPa to emphasize significant regions of accumulated stress. White dashed lines represent locations of acquired across-fault model profiles plotted in Figure 3: (A-A') length-averaged rupture trace of an estimated ∼1690 event [*Shifflett et al.*, 2002] and regional location of an estimated penultimate event of ∼1350 along the Coachella segment [*Sieh and Williams*, 1990; *Fumal et al.*, 2002]; (B-B') approximate epicenter of the 1857 Fort Tejon earthquake and regional location of an estimated penultimate event of ∼1278 [*Young et al.*, 2002]; (C-C') approximate epicenter of the 1906 San Francisco earthquake and regional location of an estimated penultimate event of 1711 [*Kelson et al.*, 2006].

that the amount of coseismic slip for each event is equal to the accumulated slip deficit on that segment, estimated by the slip rate and the time since the last major event.

3. Coulomb Stress Models

[5] Coulomb stress (σ_f), a quantitative measurement of shear (τ) and normal (σ_n) stresses acting on a fault plane
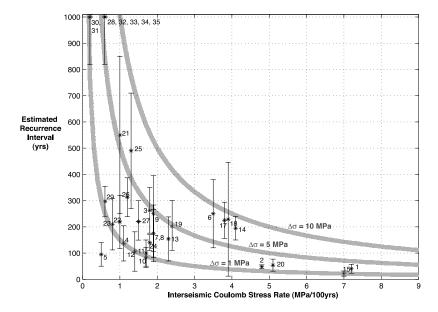
[*King et al.*, 1994], can be used to evaluate a fault's stressing behavior throughout the earthquake cycle. In this study, we calculate both Coulomb stress accumulation rate, or $\dot{\sigma}_f = \dot{\tau} - \mu_f \dot{\sigma}_n$ (where μ_f is the effective coefficient of friction), and Coulomb stress change to simulate both secular and time-variable Coulomb stress at seismogenic depth (Figure 1) (see auxiliary material). These stress calculations include updated slip rates, locking depths, and additional fault segments in the Eastern California Shear Zone (ECSZ), Death Valley, Owens Valley, and on Elsinore and Laguna Salada faults in comparison to our previous studies [e.g., *Smith and Sandwell*, 2003, 2006].

[6] Coulomb stress accumulation rate (Figure 1a) is primarily dependent on, and fairly well resolved by, interseismic GPS velocities (see auxiliary material); these stress rates do not depend on a prescribed earthquake history, nor are they sensitive to viscoelastic rheology, and therefore, we believe that these stress accumulation estimates are robust. To further justify this assessment, we compare our stress accumulation rates for a large region of Southern California with a recently published stress-rate map derived from interpolation and differentiation of GPS displacements [*Freed et al.*, 2007]. In general, the peak stress rates from our deep-slip model (presented in MPa/100yrs) are similar to, or lower than, the stresses from the *Freed et al.* [2007] model (presented in kPa/yr). The main difference, as noted by *Freed et al.* [2007], is that the stress rate of our model is more concentrated near the fault than the *Freed et al.* [2007] model. The concentration near the fault could be due to the fact that the spatial density of the GPS velocity points is not sufficient to resolve scales less than about 50 km in some places. In general, the two approaches agree within about a factor of two to five.

[7] In contrast, we find that estimates of accumulated Coulomb stress on fault segments spanning multiple earthquake cycles (Figure 1b) are not robust and are highly dependent upon the prescribed slip history of each fault segment. Lacking better information, we assume complete slip (or stress) release following each earthquake event, which will tend to provide a minimum estimate of accumulated Coulomb stress at a given time. Moreover, it should be emphasized that these are estimates of stress change and they do not reflect the absolute level of stress, which is dependent on the non-linear rheology of the crust and mantle [*Hetland and Hager*, 2005].

4. Coulomb Stress Accumulation Rate and Earthquake Recurrence Interval

[8] Segment-averaged stress accumulation rates (Figure 1a, also see auxiliary material) range from 0.2 to 7.2 MPa/100yrs, reflecting variations in slip rate, fault orientation, and locking depth. Stress accumulation rate is proportional to slip rate and is modulated by the orientation of the fault with respect to the relative velocity vector across the plate boundary. Restraining bends, such as the Big Bend region (Mojave segment 12), have higher normal stress, which increases fault friction, thus reducing the Coulomb stress. However, perhaps the most important factor in modulating stress accumulation rate is the locking depth. For example, the Imperial, Brawley, Parkfield and S. Calaveras faults (segments 1, 2, 15, 20) have shallow locking depths (<10 km) and are releasing-oriented with

Figure 2. Published recurrence intervals (see auxiliary material) of the SAFS, Δt, verses Coulomb stress accumulation rate (this study). Error bars represent combined published estimates and uncertainty ranges. Segment numbers are labeled according to Figure 1a. Segments 28 and 30–35 are suspected to have ruptured in the late Holocene [*Rockwell et al.*, 2000] and are assigned an artificial recurrence time of 1000 yrs for plotting purposes. Three characteristic stress drops are shown as thick gray lines, derived from the equation $\Delta t = \Delta\sigma/\dot\sigma_f$, reflecting constant stress drops of $\Delta\sigma = 1$, 5, and 10 MPa.
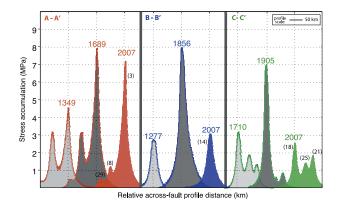
respect to the plate motion vector. These segments have relatively high rates of Coulomb stress accumulation (~5–7 MPa/100yr). Alternatively, more deeply locked fault segments (>20 km) with restraining-orientation geometry, such as the San Bernardino and Mojave faults (segments 5, 12), have lower rates of Coulomb stress accumulation (<1.5 MPa/100yr). Moreover, there is a correlation between locking depth and fault orientation suggesting that tectonically induced normal stress may have an important influence on depth-averaged fault strength.

[9] The wide range of Coulomb stress accumulation rates along the SAFS enables us to test the validity of the periodic (or characteristic) model of the earthquake cycle [*Reid*, 1910]. We compare independent estimates of earthquake recurrence interval (including uncertainties) [*Working Group on California Earthquake Probabilities* (*WGCEP*), 1995, 2003, 2007; *Weldon et al.*, 2005] to fault-averaged Coulomb stress accumulation rates and observe an inverse relationship (Figure 2). Fault segments having high stress accumulation rate (>4 MPa/100yr) generally have shorter recurrence intervals, while faults with low stress accumulation rate (<1.5 MPa/100yr) generally have longer recurrence intervals. In particular, the Imperial, Brawley, Parkfield, and S. Calaveras segments have recurrence intervals of less than 60 years and high Coulomb stress accumulation rates. In contrast, the N. Calaveras, Elsinore, and ECSZ faults (segments 21, 29, 30–35) have longer recurrence intervals and moderate to low Coulomb stress accumulation rates. There are, however, some notable exceptions such as the Cholame and SAF Peninsula regions (segments 14, 18), where model-implied stress drops are as large as 9 MPa, and which have failed in the two largest recorded earthquakes in California history (M7.9 1857 Fort Tejon earthquake, M7.8 1906 San Francisco earthquake). Rates for the Superstition Hills fault

(segment 6) also suggests an anomalously large stress drop per event, however the paleoseismic record of this segment is poorly known, further complicated by sporadic creeping events [*Wei et al.*, 2009], which may reduce stress.

[10] The observed relationship between recurrence interval and Coulomb stress accumulation rate highlights three important issues. First, accumulated stress per fault segment (0.2–7.2 MPa/100yrs) is consistent with seismically observed stress drops from major strike-slip earthquakes [*Brace and Byerlee*, 1996]. Second, stress accumulation rate is proportional to slip rate and inversely proportional to locking depth. Therefore, it is important to accurately measure the effective locking depth of a fault to understand along-strike variations in stress. Third, the recurrence interval data, including uncertainties, are inconsistent with a uniform stress drop per major event for all segments of the SAFS. This failure of the characteristic model may indicate that the absolute level of Coulomb stress along these faults is greater than the seismic stress drop.

5. Present-Day Stress Accumulation and Historical Stress Thresholds

[11] A much more speculative application of this model is the calculation of time variations in Coulomb stress on each fault segment (Figure 1b, also see auxiliary material). To first order, the modeled stress on each fault segment is equal to the stress accumulation rate times the time since the last major earthquake. Second order effects include loading from sub-parallel faults and viscoelastic residual effects from prior earthquakes. For calendar year 2007, regions of relatively low stress accumulation include the Superstition Hills, Borrego, Parkfield, Santa Cruz Mountains, and S. Calaveras faults (segments 6, 7, 15, 17, 20) where there

Figure 3. Across-fault stress profiles based on historical and prehistorical earthquake activity of the SAFS. Profile A-A′ (red) crosses the southern SAFS region (see Figure 1b, segments 29, 8, 3); profile B-B′ (blue) crosses the central SAFS (segment 14); profile C-C′ (green) crosses the northern SAFS (segments 18, 21, 25). Stresses are computed for calendar year 2007 (solid color profiles), as well for the years just prior to the most recent event (dark gray fill) and the penultimate event (light gray fill). Multiple peaks per profile represent stress levels on paralleling fault segments (labeled on the 2007 profile for each region) at the indicated observational year.

has either been a recent earthquake (within the last 20 years), or Coulomb stress accumulation rate is low due to fault geometry and locking depth. Alternatively, regions of relatively high stress accumulation include most of the southern San Andreas from Coachella (segment 3) to Cholame (segment 14), the Anza portion of the San Jacinto fault (segment 9), and along the eastern Bay Area (segment 24).

[12] Despite uncertainties in paleoseismic chronologies, it is instructive to estimate stress accumulation prior to the most recent large events ("hindcast" modeling) and compare these with present-day modeled stress accumulation. We compare across-fault profiles of historical stress accumulation for three example regions (Figures 1b and 3). Note that local stress maxima coincide with the traces of the major fault segments. Stress is high prior to major ruptures (4−8 MPa), however we again emphasize that the level of stress is essentially prescribed by the assumed slip history. The northern SAFS (C-C′) shows present-day stress levels that are currently much lower than accumulated stress prior to the recorded 1906 event (~7 MPa) and the penultimate 1711 event [*Kelson et al.*, 2006] (~3.3 MPa). Likewise, the present-day stress level on the central SAFS (B-B′) appears to be much lower than stress prior to the 1857 event (~7.9 MPa), however larger than an estimated event in 1278 [*Young et al.*, 2002] (~2.6 MPa). In contrast, the southern SAFS (A-A′) region has stress levels that are approaching the level prior to an estimated 1690 rupture [*Shifflett et al.*, 2002] (~7.8 MPa), and much greater than the stress prior to an estimated penultimate event of 1350 [*Sieh and Williams*, 1990; *Fumal et al.*, 2002] (~4.6 MPa).

6. Conclusions and Implications

[13] The stress modeling results presented here have important implications for seismic hazard analyses, however

it is important to consider other factors that may alter the state of stress (i.e., aseismic creep at depth [*Burgmann et al.*, 2000], local variations in pore fluid pressure [*Peltzer et al.*, 1996], dynamic stress changes due to earthquake rupture [*Olsen et al.*, 1997], and failure according to rate and state friction laws [*Tse and Rice*, 1982]). The model discussed here only considers the changes in stress due to earthquake kinematics and cannot be used to estimate the absolute level of stress due to long-term sliding and dilatation. The model also introduces several geologic simplifications to the earthquake cycle, whereas strain accumulation and release rate may vary over time [*Bennett et al.*, 2004]. Furthermore, determining how "characteristically" each fault segment behaves over multiple earthquake cycles depends on a reliable record of prehistorical events.

[14] Nevertheless, because stress drops of major strike-slip earthquakes are on the order of 10 MPa [*Brace and Byerlee*, 1996; *Beeler et al.*, 2001], these first-generation models may provide a lower bound on estimates of stress evolution throughout the historical era, and perhaps an upper bound on the expected recurrence interval of a particular fault segment. Even more importantly, they highlight the need for a more comprehensive paleoseismic database. While more rheologically complex models should be considered in the future, these current models provide an important tool for qualitative interpretation and analysis of plate boundary stress evolution of the SAFS.

References

Becker, T. W., J. Hardebeck, and G. Anderson (2004), Constraints on fault slip rates of the southern California plate boundary from GPS velocity and stress inversions, *Geophys. J. Int.*, 160, 634–650, doi:10.1111/j.1365-246.

Beeler, N. M., S. H. Hickman, and T. F. Wong (2001), Earthquake stress drop and laboratory-inferred interseismic strength recovery, *J. Geophys. Res.*, 106, 30,701–30,713.

Bennett, R. A., A. M. Friedrich, and K. P. Furlong (2004), Co-dependent histories of the San Andreas and San Jacinto fault zones from inversion of geologic displacement rate data, *Geology*, 32, 961–964.

Brace, W. F., and J. D. Byerlee (1996), Stick-slip as a mechanism for earthquakes, *Science*, 153, 990–992.

Burgmann, R., D. Schmidt, R. M. Nadeau, M. d'Alessio, E. Fielding, D. Manaker, T. V. McEvilly, and M. H. Murray (2000), Earthquake potential along the northern Hayward fault, California, *Science*, 289, 1178–1182.

Eberhart-Phillips, D., M. Lisowski, and M. D. Zoback (1990), Crustal strain near the Big Bend of the San Andreas fault: Analysis of the Los Padres-Tehachapi trilateration networks, California, *J. Geophys. Res.*, 95, 1139–1153.

Fay, N. P., and E. D. Humphreys (2005), Fault slip rates, effects of elastic heterogeneity on geodetic data, and the strength of the lower crust in the Salton Trough region, southern California, *J. Geophys. Res.*, 110, B09401, doi:10.1029/2004JB003548.

Freed, A. M., S. T. Ali, and R. Burgmann (2007), Evolution of stress in southern California for the past 2000 years from coseismic, postseismic and interseismic stress changes, *Geophys. J. Int.*, 169, 1164–1179.

Fumal, T. E., M. J. Rymer, and G. G. Seitz (2002), Timing of large earthquakes since AD 800 on the Mission Creek strand of the San Andreas fault zone at Thousand Palms Oasis, near Palm Springs, California, *Bull. Seismol. Soc. Am.*, 92, 2841–2860.

Grant, L. B., and W. R. Lettis (2002), Introduction to the special issue on paleoseismology of the San Andreas fault system, *Bull. Seismol. Soc. Am.*, 92, 2552–2554.

Hetland, E. A., and B. H. Hager (2005), Postseismic and interseismic displacements near a strike-slip fault: A two-dimensional theory for general linear viscoelastic rheologies, *J. Geophys. Res.*, *110*, B10401, doi:10.1029/2005JB003689.

Kelson, K. K., A. R. Streig, R. D. Koehler, and K. Kang (2006), Timing of late Holocene paleoearthquakes on the northern San Andreas fault at the Fort Ross orchard site, Sonoma County, California, *Bull. Seismol. Soc. Am.*, *96*, 1012–1028, doi:10.1785/0120050123.

King, G. C. P., R. S. Stein, and J. Lin (1994), Static stress changes and the triggering of earthquakes, *Bull. Seismol. Soc. Am.*, *84*, 935–953.

Lyons, S. N., Y. Bock, and D. T. Sandwell (2002), Creep along the Imperial fault, southern California, from GPS measurements, *J. Geophys. Res.*, *107*(B10), 2249, doi:10.1029/2001JB000763.

Meade, B. J., and B. H. Hager (2005), Block models of crustal motion in southern California constrained by GPS measurements, *J. Geophys. Res.*, *110*, B03403, doi:10.1029/2004JB003209.

Murray, J. R., and P. Segall (2002), Testing time-predictable earthquake recurrence by direct measure of strain accumulation and release, *Nature*, *419*, 287–291.

Olsen, K. B., R. Madariaga, and R. J. Archuleta (1997), Three-dimensional dynamic simulation of the 1992 Landers earthquake, *Science*, *278*, 834–838.

Parsons, T. (2006), Tectonic stressing in California modeled from GPS observations, *J. Geophys. Res.*, *111*, B03407, doi:10.1029/2005JB003946.

Peltzer, G. P., P. Rosen, F. Rogez, and K. Hudnut (1996), Postseismic rebound in fault step-overs caused by pore fluid flow, *Science*, *273*, 1202–1204.

Reid, H. F. (1910), *The California Earthquake of April 18, 1906: Report of the State Earthquake Investigation Committee*, vol. 2, *The Mechanics of the Earthquake, Carnegie Inst. Washington Publ., 87*.

Rockwell, T. K., S. Lindvall, M. Herzberg, D. Murbach, T. Dawson, and G. Berger (2000), Paleoseismology of the Johnson Valley, Kickapoo, and Homestead Valley faults: Clustering of earthquakes in the eastern California shear zone, *Bull. Seismol. Soc. Am.*, *90*, 1200–1236, doi:10.1785/0119990023.

Shen, Z. K., D. C. Agnew, and R. W. King (2003), The SCEC Crustal Motion Map, version 3.0, South. Calif. Earthquake Cent., Los Angeles. (Available at http://epicenter.usc.edu/cmm3)

Shifflett, H., M. G. Gray, R. Grannell, and B. L. Ingram (2002), New evidence on the slip rate, renewal time, and late Holocene surface displacement, southernmost San Andreas fault, Mecca Hills, *Bull. Seismol. Soc Am.*, *92*, 2861–2877.

Sieh, K. E., and P. L. Williams (1990), Behavior of the southernmost San Andreas fault during the past 300 years, *J. Geophys. Res.*, *95*, 6629–6645.

Smith, B., and D. Sandwell (2003), Coulomb stress accumulation along the San Andreas fault system, *J. Geophys. Res.*, *108*(B6), 2296, doi:10.1029/2002JB002136.

Smith, B., and D. Sandwell (2004), A three-dimensional semianalytic viscoelastic model for time-dependent analyses of the earthquake cycle, *J. Geophys. Res.*, *109*, B12401, doi:10.1029/2004JB003185.

Smith, B. R., and D. T. Sandwell (2006), A model of the earthquake cycle along the San Andreas Fault System for the past 1000 years, *J. Geophys. Res.*, *111*, B01405, doi:10.1029/2005JB003703.

Tse, S. T., and J. R. Rice (1982), Crustal earthquake instability in relation to the depth variation of frictional slip properties, *J. Geophys. Res.*, *91*, 9452–9472.

Wdowinski, S., B. Smith-Konter, Y. Bock, and D. T. Sandwell (2007), Spatial characterization of the interseismic velocity field in southern California, *Geology*, *35*, doi:10.1130/G22938A.1.

Wei, M., D. Sandwell, and Y. Fialko (2009), A silent M w 4.7 slip event of October 2006 on the Superstition Hills fault, southern California, *J. Geophys. Res.*, *114*, B07402, doi:10.1029/2008JB006135.

Weldon, R., T. Fumal, and G. Biasi (2004), Wrightwood and the earthquake cycle: What a long recurrence record tells us about how faults work, *GSA Today*, *14*, 4–10, doi:10.1130/1052–5173.

Weldon, R., T. Fumal, G. Biasi, and K. Scharer (2005), Past and future earthquakes on the San Andreas fault, *Science*, *308*, 966–967, doi:10.1126/science.1111707.

Working Group on California Earthquake Probabilities (WGCEP) (1995), Seismic hazards in southern California: Probable earthquakes, 1994 to 2024, *Bull. Seismol. Soc. Am.*, *85*, 379–439.

Working Group on California Earthquake Probabilities (WGCEP) (2003), Earthquake probabilities in the San Francisco Bay region: 2002–2031, *U.S. Geol. Surv. Open File Rep.*, *03–214*.

Working Group on California Earthquake Probabilities (WGCEP) (2007), The uniform California earthquake rupture forecast, version 2, *U.S. Geol. Surv. Open File Rep.*, *2007-1437*.

Young, J. J., J. R. Arrowsmith, L. Colini, L. B. Grant, and B. Gootee (2002), Three-dimensional excavation and recent rupture history along the Cholame segment of the San Andreas fault, *Bull. Seismol. Soc. Am.*, *92*, 2670–2688.

_____

D. Sandwell, Institute for Geophysics and Planetary Physics, Scripps Institution of Oceanography, 9500 Gilman Drive, La Jolla, CA 92093-0225, USA. (dsandwell@ucsd.edu)

B. Smith-Konter, Department of Geological Sciences, University of Texas at El Paso, 500 West University Drive, El Paso, TX 79968-0555, USA. (brkonter@utep.edu)